

Accounts

Multi-Dimensional Crystal Structures and Unique Solid-State Properties of Heterocyclic Thiazyl Radicals and Related Materials

Kunio Awaga,*[1] Toshiyuki Tanaka,[1] Takahiro Shirai,[1] Masato Fujimori,[1] Yosuke Suzuki,[1] Hirofumi Yoshikawa,[1] and Wataru Fujita*[2]

[1]Department of Chemistry, Graduate School of Science, Nagoya University, Chikusa-ku, Nagoya 464-8602

[2]Research Center of Materials Science, Nagoya University, Chikusa-ku, Nagoya 464-8602

Received May 2, 2005; E-mail: awaga@mbox.chem.nagoya-u.ad.jp

The crystal structures and magnetic properties of heterocyclic thiazyl radicals and related materials have been examined. TTTA (=1,3,5-trithia-2,4,6-triazapentalenyl) exhibited a first-order phase transition between a paramagnetic high-temperature (HT) phase and a diamagnetic low-temperature (LT) phase, with a wide thermal hysteresis loop over the temperature range 230–305 K. The phase control of TTTA was achieved by pressure and by light irradiation. BDTA (=1,3,2-benzodithiazolyl) also exhibited a diamagnetic–paramagnetic phase transition above room temperature. However, fresh samples always exhibited a superheating of the LT phase that resulted in a double melting (melt–recrystallization–melt process) and supercooling of the HT phase, which in turn led to an antiferromagnetic ordering at 11 K. The molecular compounds of thiazyl radicals were prepared; TTTA formed a coordination polymer structure in the TTTA·[Cu(hfac)$_2$ (=bis(hexafluoroacetylacetonato)–copper(II))] crystal, where a ferromagnetic coupling was found between the organic and inorganic species. The cation radical salts, [BBDTA (=benzo[1,2-*d*:4,5-*d*′]bis[1,3,2]dithiazole)]·MCl_4 (M = Ga and Fe), exhibited ferromagnetic ordering at 7 K and ferrimagnetic ordering at 44 K after evaporation of crystal solvents. We also grew crystals of M–TTDPz (TTDPz = tetrakis(thiadiazole)porphyrazine and M = H_2, Fe, Co, Ni, Cu, and Zn) and performed their structural analyses. Their crystal structures were found to depend strongly on the central metal ion and could be classified into three forms: α, β, and γ.

The electrical and magnetic properties of molecular crystals have been studied extensively in the past three decades, and various molecule-based conductors, superconductors, and magnetic materials have been synthesized to date. The research has been characterized by the enhancement of dimensionality in intermolecular interactions. The first molecular metal, TTF–TCNQ, exhibited a Peierls transition due to instability of the 1D conducting pathway formed by the π–π overlap.[1] Increasing the dimensionality to overcome the 1D instability led to the discovery of molecular superconductors, such as the TMTSF and BEDT-TTF series.[1] More recent examples include the fullerene conductors, e.g. K_xC_{60}, in which C_{60} has a 3D interaction.[2] A similar materials development history is observed in the case of molecule-based magnetic materials. While the galvinoxyl radical, whose ferromagnetic interaction was found in the 1960's, exhibited a spin-Peierls-like transition, upon which it lost its ferromagnetic properties,[3] the first organic ferromagnet, *p*-NPNN, possessed a 3D network structure.[4]

Heterocyclic thiazyl radicals possess unique chemical and physical properties.[5] They can be regarded as being on the borderline between organic and inorganic materials. They are chemically stable, in contrast to the instability of most organic radicals, so that they do not need protection groups on their molecular skeletons. This brings about a close packing in the solid state. Their molecular skeletons exhibit a large electronic polarization, leaving, respectively, a positive and a negative polarized charge on sulfur and nitrogen. These charges form short intermolecular and interatomic S···N contacts. Thiazyl radical solids always involve a multi-dimensional network consisting of face-to-face π–π overlaps and side-by-side S···N contacts. They have a strong spin–lattice interaction; a small lattice modification brings about a significant change in their magnetism, reflecting the fact that the SOMO (singly occupied molecular orbital) has a phase change between bonded sulfur and nitrogen. These interesting characteristics are believed to provide them with their unique solid-state physical properties (Chart 1).

Room-Temperature Magnetic Bistability in TTTA

Magnetic Properties. TTTA was synthesized by Wolmershäuser and Johann in 1989.[6] Recently, it was found that TTTA exhibits a first-order phase transition with a surprisingly wide thermal hysteresis loop around room temperature.[7] Figure 1a depicts the temperature dependence of the paramagnetic susceptibility χ_p for a polycrystalline sample of TTTA. The bold arrow in this figure indicates the value of χ_p for the virgin sample just after sublimation crystallization. As the

Published on the web January 13, 2006; DOI 10.1246/bcsj.79.25

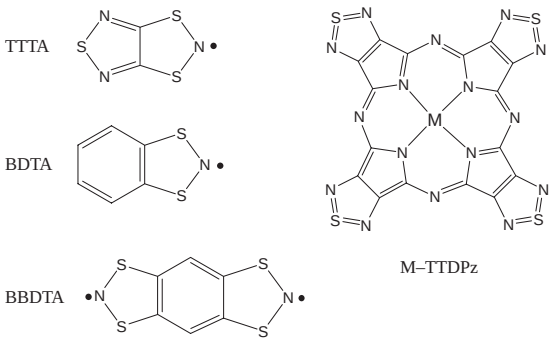

Chart 1.

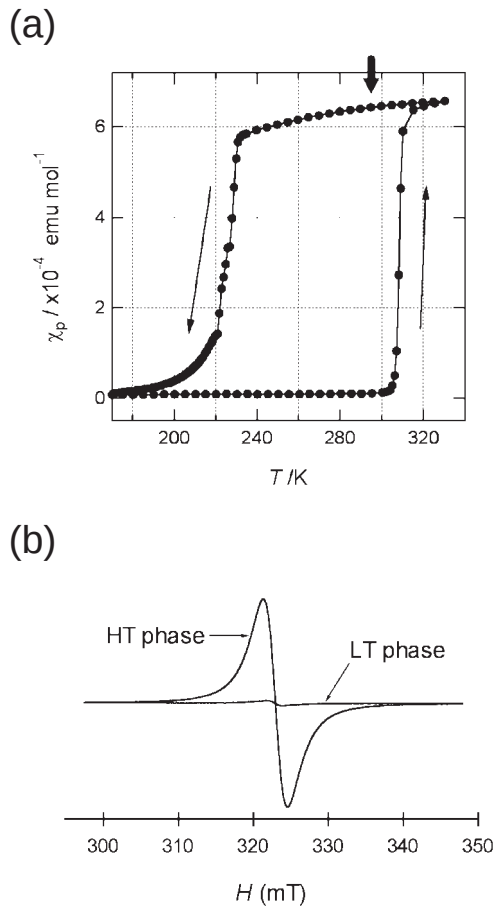

Fig. 1. (a) Temperature dependence of the paramagnetic susceptibility χ_p for a polycrystalline sample of TTTA. The bold arrow indicates the χ_p value for the virgin sample just after sublimation. (b) X-band EPR spectra of the HT and LT phases of TTTA at room temperature.

sample was cooled from room temperature, χ_p showed a slight decrease. In this temperature range, the value of $\chi_p T$ was ca. 0.2 emu K mol^{-1}, which was much smaller than that of the Curie spin. This is probably caused by a 3D antiferromagnetic interaction in the crystal of TTTA. At $T_{c\downarrow} = 230$ K, χ_p began to decrease rapidly, becoming zero at 170 K; TTTA is intrinsically diamagnetic at low temperatures. When the sample was heated from a low temperature, a diamagnetic-to-paramagnetic transition was found at $T_{c\uparrow} = 305$ K, indicating the large hysteresis loop. Since this loop goes through room temperature (290 K), TTTA is regarded as a magnetically-bistable material at room temperature. There was little change in the shape of the loop even after repeats of this thermal cycle.

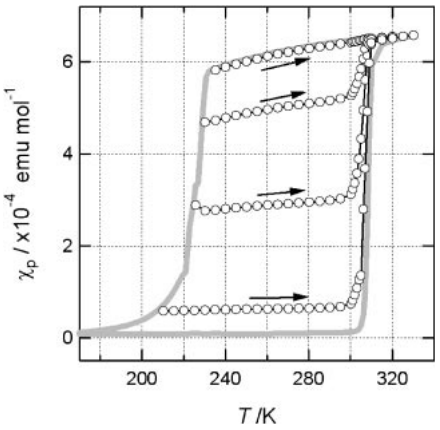

Fig. 2. The magnetic response of TTTA at $T_{c\downarrow}$ to increases in temperature. The four plots represent results on samples with different starting points. The bold gray curves depict the hysteresis loop shown in Fig. 1a.

To prove that the hysteresis loop observed is intrinsic, we carried out the following experiments. The high-temperature (HT) phase was slowly cooled from room temperature to 230 K ($T_{c\downarrow}$). The cooling was stopped during the phase transition to the diamagnetic low-temperature (LT) phase. Subsequently, the sample was heated; during this process, the magnetic response was monitored. The results for four runs with different starting points are depicted in Fig. 2.[8] In every run, the χ_p plots clearly indicated that there was little change in the ratio between the HT and LT phases in the temperature range within the loop. This indicated that the two phases coexisted stably in this range, providing firm evidence that the hysteresis was intrinsic at least in the time scale of laboratory experiments.

Organic radicals are usually EPR active so that we can obtain precise spin information through high-sensitivity EPR measurements. The temperature-variable X-band EPR experiments indicated the phase transition of TTTA at ca. 200 and 310 K upon cooling and heating, respectively.[8] Figure 1b compares the single-crystal EPR signals for the two phases at 300 K. The spectrum of the HT phase reveals an intense absorption, in contrast to the weak signal of the LT phase. The *g*-factor of the HT phase signal is $\bar{g} = 2.0043$, which is typical for thiazyl radicals. Since EPR is highly sensitive to the spin state of organic radicals, the two phases of TTTA can be very easily distinguished by EPR, rather than SQUID measurements.

Crystal Structures. TTTA exhibited a significant difference between the crystal structures of the HT and LT phases.[7,8] The HT phase crystallized in the monoclinic $P2_1/c$ space group. The structure consisted of a polar 1D stacking column, in which the molecules were related by translational relations with a constant interval. This stacking column was surrounded by six neighboring columns with very short S···N and S···S contacts. By contrast, TTTA exhibited a strong dimerization along the stacking direction in the crystal structure of the LT phase that belonged to the triclinic $P\bar{1}$ space group. This radi-

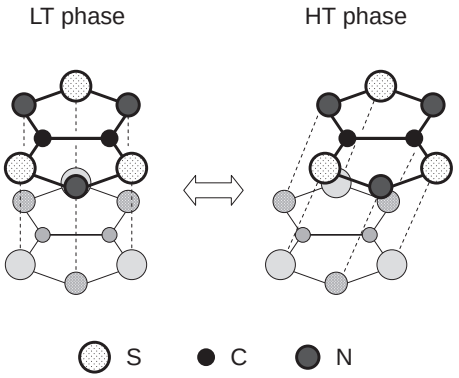

Fig. 3. Nearest neighbor intermolecular overlaps of TTTA in the HT and LT phases. The electrostatic interaction favors a shifted overlap, while the exchange interaction results in an eclipsed overlap.

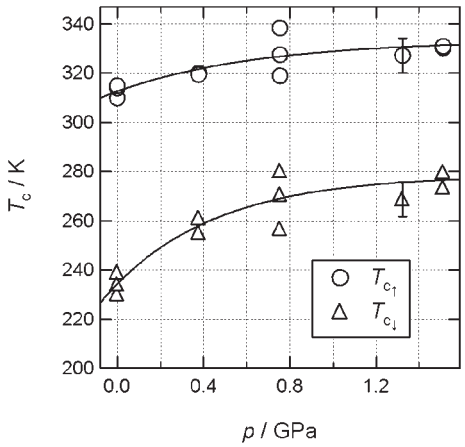

Fig. 4. Pressure dependence of the transition temperatures, $T_{c\downarrow}$ and $T_{c\uparrow}$, for TTTA. Solid curves are eye guides.

cal dimerization must be responsible for the diamagnetic properties of the LT phase. Figure 3 shows a schematic comparing the nearest neighbor intermolecular arrangements in the two phases. It was notable that the molecules had an eclipsed overlap in the LT phase, in contrast to a shifted overlap in the HT phase. More specifically, the molecular planes in the LT-phase dimer were not parallel; the distance between the –S–N–S– moieties was shorter by ca. 0.09 Å than that between the –N–S–N– moieties, probably reflecting a bonding interaction between the unpaired electrons which were concentrated on the –S–N–S– moieties. This suggests that bond formation is the main driving force of this phase transition.

We believe that there is a competition between the exchange and electrostatic interactions (see Fig. 3). The exchange interaction favors an eclipsed overlap, such as that found in the LT phase, because this structure maximizes the intermolecular overlap between the SOMOs. However, this is the most disagreeable structure from the viewpoint of electrostatic energy because it includes intermolecular and interatomic contacts between polarized charges of the same sign, namely $S^{\delta+}\cdots S^{\delta+}$ and $N^{\delta-}\cdots N^{\delta-}$. It is presumably this competition that causes the drastic phase transitions in the thiazyl radical family.

Thermodynamic Properties and Phase Control. The phase transition of TTTA was examined by means of DSC.[8] In the cooling and the heating process, exothermic and endothermic transitions were observed at 234 and 315 K (on-set temperatures), respectively. The transition enthalpy ΔH values at $T_{c\downarrow}$ and $T_{c\uparrow}$ were determined to be 2210 and 2340 J mol^{-1}, respectively. The difference must be due to the fact that the HT and LT phases have different heat capacities. The transition entropies ΔS upon cooling and heating were estimated to be $\Delta S_\downarrow = \Delta H_\downarrow / T_{c\downarrow} = 9.44$ J K^{-1} mol^{-1} and $\Delta S_\uparrow = \Delta H_\uparrow / T_{c\uparrow} = 7.43$ J K^{-1} mol^{-1}, respectively. While the maximum estimation of the magnetic contribution is $R\ln 2$ (=5.76 J K^{-1} mol^{-1}), the real contribution would be smaller than $R\ln 2$ because the HT phase involves rather strong antiferromagnetic interactions. Nevertheless, the ΔS values observed are larger than the maximum estimation. The excess entropy indicates involvement of the lattice system in the phase transition.

The effects of quasi-hydrostatic pressures on TTTA were studied to control the magnetic bistability. Despite extensive studies on the effects of high pressure on molecular crystals, non-equilibrium phenomena, namely hysteresis behavior, remain largely unexplored.[9–11] The temperature dependence of χ_p of TTTA was studied under 0.38, 0.75, and 1.5 GPa.[12] TTTA was found to undergo a sharp diamagnetic–paramagnetic transition even under pressure, with a significant shift in the transition temperature. The pressure dependences of $T_{c\uparrow}$ and $T_{c\downarrow}$ are shown in Fig. 4. Both $T_{c\uparrow}$ and $T_{c\downarrow}$ increased significantly with increasing pressure. Thus, the bistable range shifted toward higher temperatures. Although room temperature (290 K) is just below $T_{c\uparrow}$ at ambient pressure, it falls in the center of the hysteresis loop at 0.75 GPa. That is, room-temperature bistability can be stabilized by pressure. The two solid curves in Fig. 4 are only eye guides, but the gradients at the ambient pressure are estimated to be roughly $dT_{c\downarrow}/dp = 45 \pm 20$ K GPa^{-1} and $dT_{c\uparrow}/dp = 20 \pm 10$ K GPa^{-1}. The theoretical value of dT_c/dp is given by the Clapeyron equation, $dp/dT_c = \Delta S/\Delta V = \Delta H/(T_c \Delta V)$, where ΔV is the volume change, though this equation is valid only under thermal equilibrium. The enthalpy changes for the transitions in TTTA were obtained by DSC measurements, as described above. The difference between the unit cell volumes of the two phases is 3.4 Å^3 at room temperature.[7,8] Since the unit cell contains four molecules, the volume difference is $\Delta V_{RT} = 3.4 N_A/4$ Å^3 mol^{-1}, where N_A is Avogadro's constant. The theoretical value for dT_c/dp at $p = 0$ GPa can be estimated to be 60 K GPa^{-1} under the assumption that $\Delta V = \Delta V_{RT}$. The agreement between the theoretical and experimental values is fairly good (the same order of magnitude), and the equation can explain the shift toward higher transition temperatures with increasing pressure.

The phase control of TTTA was achieved using photoirradiation.[13] There is a very clear chromism between the crystal surfaces of the two phases under a polarized microscope, namely between red-purple in the HT phase and yellow-green in the LT phase. The photo-induced transition from the diamagnetic LT phase to the paramagnetic HT phase was observed after a single-shot (6 ns pulse) irradiation at 2.64 eV at 296 K. In addition, a clear threshold was identified in the dependence of the LT-to-HT conversion efficiency on the excitation photon density. This strongly indicated that the observed was not a thermal

effect, but a photo-induced phase transition.[13]

Magnetic Bistability in Molecule-Based Materials. In some recent studies of molecule-based materials, bistable materials have been discovered in materials ranging from molecules to liquid crystals and solid-state materials. The most spectacular examples include the spin-crossover complexes, i.e. $[Fe(phy)_2](BF_4)_2$ (phy = 1,10-phenanthroline-2-carbaldehydephenylhydrazone), which exhibits this transition between $S = 0$ and $S = 2$, with a large thermal hysteresis.[14] The pressure effects on this compound were examined up to 0.4 GPa, and a shift of the bistable range to higher temperatures was observed with $dT_c/dp = 30\,K\,GPa^{-1}$ (the average of $dT_{c\uparrow}/dp$ and $dT_{c\downarrow}/dp$). Now we will compare the pressure effects on this spin-crossover complex with those on TTTA. The dT_c/dp value for the Fe(II) complex is similar to that for TTTA. In $[Fe(phy)_2](BF_4)_2$, the volume change between the two phases is $15N_A$ Å^3 mol^{-1}, while that of TTTA is $3.4N_A/4$ Å^3 mol^{-1}. Thus, by the Clapeyron equation, the volume term leads to a greater increase in dT_c/dp for $[Fe(phy)_2](BF_4)_2$ compared to that in TTTA. The entropy change of the spin-crossover transition is moderate ($85\,J\,K^{-1}\,mol^{-1}$) because it includes the spin contribution $R\ln 5$ caused by the change from $S = 0$ to 2. By contrast, the spin contribution to the transition entropy of TTTA is smaller than $R\ln 2$ ($=5.76\,J\,K^{-1}\,mol^{-1}$) because the transition in TTTA occurs between a diamagnetic phase and a "suppressed" paramagnetic phase due to antiferromagnetic intermolecular interactions. As such, the small spin contribution is believed to be responsible for the small TTTA entropy change, namely $8.4\,J\,K^{-1}\,mol^{-1}$ (the average of $\Delta S_\uparrow$ and $\Delta S_\downarrow$), which likely leads to a high sensitivity to pressure. The transitions in TTTA and $[Fe(phy)_2](BF_4)_2$ exhibit similar shifts to higher temperatures with increasing pressure, but the origins are probably very different.

Charge Doping. The electrical properties of TTTA were examined. The conductivity for the HT phase was 10^{-8} Ω^{-1} cm^{-1}, with an activation energy of 0.33 eV under vacuum. The conductivity for the LT phase was two orders of magnitude lower. The HT phase was found to be an insulator despite its three-dimensional network structure free of radical dimerization, where each molecule has one unpaired electron. Thus, it is highly possible that the HT phase can be regarded as a Mott insulator: Strong on-site electron–electron repulsion results in electron localization.

The carrier doping on the HT phase of TTTA was carried out with I_2 vapor. Figure 5 depicts the time dependence of the conductivity, measured by the two-probe method during doping. The conductivity σ was quickly enhanced by four or five orders of magnitude, saturating after 10 h. The saturation was presumably due to a breakup of the crystal structure caused by penetration of the dopant. Since the doped material was very air-sensitive, we could not carried out further characterization. It was clearly demonstrated, however, that hole doping of the HT phase of TTTA brought about significant enhancement of the conductivity.

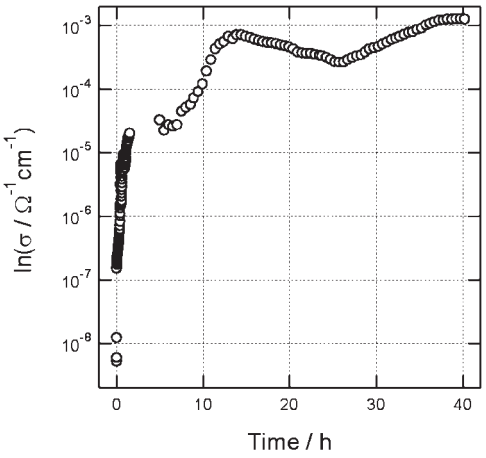

Fig. 5. Time dependence of the conductivity of TTTA during I_2 doping.

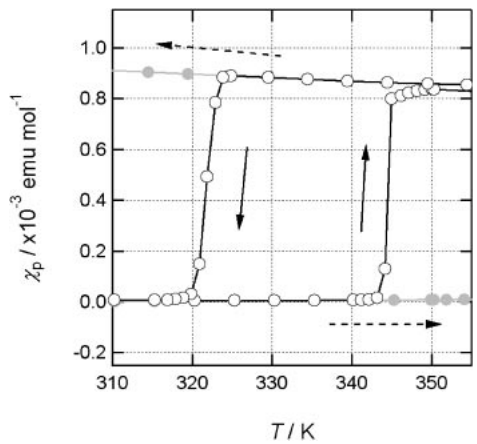

Fig. 6. Temperature dependence of χ_p for BDTA above room temperature. The gray plots indicate the effects of superheating and supercooling.

Complex Phase Transitions in BDTA: Spin-Gap, Antiferromagnetic Ordering, and Double Melting

Diamagnetic–Paramagnetic Phase Transition. The thiazyl radical 1,3,2-benzodithiazolyl (abbreviated as BDTA) was synthesized by Wolmershäuser et al. in 1984.[15] Awere et al. reported its crystal structure: It consists of a centrosymmetric dimmer, where the dimer units form a two-dimensional network with short S···S contacts.[16] This is very similar to the structure of the κ-modification of (BEDT-TTF)$_2$X (BEDT-TTF = bis(ethylenedithio)tetrathiafulvalene, X = Cu(NCS)$_2$, etc.), known as organic superconductors whose critical temperatures exceed 10 K.[17] Awere et al. also reported that BDTA was diamagnetic at least below room temperature because of strong antiferromagnetic interactions in the structure.[16] In this section, we will describe the complex phase transitions in BDTA, where a diamagnetic spin-gap phase, a paramagnetic phase, an antiferromagnetic ordered phase, and a liquid phase, interplay.[18]

Figure 6 depicts the temperature dependence of χ_p for BDTA above room temperature (open circles). BDTA was diamagnetic at room temperature due to its dimerized structure.[16] Upon heating, however, BDTA exhibited a first-order phase transition to a paramagnetic high-temperature phase at 346 K, though the structure of this phase has not yet been identified. In the cooling process, a paramagnetic-to-diamagnetic transition was observed at 320 K, which was associated with

the hysteresis of 26 K. This value is much smaller than that of TTTA, but still larger than the others in usual molecular solids. It should be noted that this transition can be observed only for the aged BDTA samples, which were subjected to repeated thermal cycles over the 2–365 K range. These cycles facilitated the phase transition, probably due to an increase in the concentration of lattice defects. Thus, fresh samples always exhibited superheating and supercooling, as described in the next section.

Superheating and Supercooling. The most characteristic feature of BDTA is the occurrence of superheating and supercooling on phase transition above room temperature. They always took place in the case of fresh BDTA samples. The magnetic behavior in these non-equilibrium processes is shown in Fig. 6 as gray circles. Figure 7 depicts the Gibbs free energy for BDTA determined by magnetic measurements and visual observation. In the figure, L and MO denote the liquid and antiferromagnetic ordered phases, respectively. The intersection between the LT and HT curves indicates the diamagnetic–paramagnetic phase transition at 346 K. Upon further heating of the superheated LT phase, the material melted at 360 K once, but the liquid immediately solidified into the HT phase even upon heating. This is because the free energies decrease in the order LT > L > HT in the 360–364 K range. Upon heating, the LT phase relaxes into the HT phase through the L phase at 360 K. At 364 K, the solid of BDTA in the HT phase exhibited a second melting. This process has been called double melting, and has been observed, for example, in molecular crystals and organic polymers.[19] It is notable that the L phase exhibited paramagnetism with χ_p of 9.0×10^{-4} emu mol^{-1} at 365 K, though further heating brought about a thermal decomposition with gas generation.

Supercooling of the HT phase also occurred (see Fig. 6) and further cooling resulted in antiferromagnetic ordering at 11 K. The temperature dependence of χ_p for the supercooled HT phase followed the Curie–Weiss law with $\theta = -93$ K and $C = 0.375$ emu K mol^{-1} (fixed), where θ and C are the Weiss and Curie constants, respectively. Below 15 K, χ_p showed a slight decrease with a rather abrupt change around 11 K, suggesting the antiferromagnetic ordering. The temperature dependence of the heat capacity c_p exhibited a λ-shaped anomaly at 11 K, supporting the antiferromagnetic ordering at this temperature. The HT phase transforms into the MO phase below 11 K, as indicated in Fig. 7. The structures of the HT and MO phases must be nearly the same. Thus, it is thought that the crystal structures for the spin-gap state and the antiferromagnetic ordered state are switched at the phase transition at 346 K.

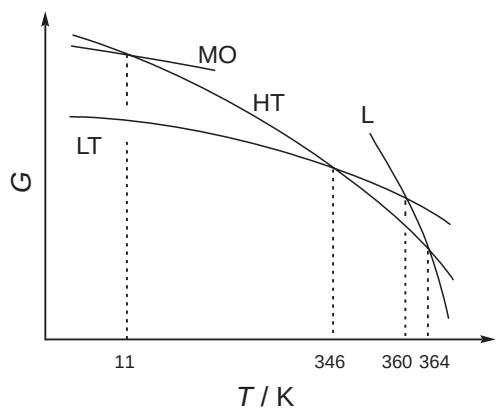

Fig. 7. Gibbs energy phase diagram for BDTA. HT: high-temperature phase; LT: low-temperature phase; L: liquid; MO: antiferromagnetic ordered state.

The complicated temperature dependence of the magnetic behavior of BDTA was clearly explained in terms of the cooperation between the double melting, solid-state phase transition and magnetic ordering, in which the HT, LT, L, and MO phases interplayed. Alternative relationships between the spin-gap state and the antiferromagnetic ordered state have been reported in low-dimensional magnetic materials, such as spin-Peierls compounds,[20] and copper-oxide high-T_c superconductors.[21] While the competition between the two states occurs on the identical crystal structure in these materials, BDTA forms two states with different crystal structures that are linked at the structural phase transition.

Ferromagnetic Coordination Polymer in TTTA·Cu(hfac)$_2$

In this section, we will describe a useful function of thiazyl radicals, namely as building blocks for supramolecular materials. As already mentioned, these radicals exhibit strong electric polarization, leaving negative charges on the nitrogens and positive charges on the sulfurs. In addition, the nitrogen atoms show basicity, so that thiazyl radicals can operate as a ligand to various metal ions.

A 1:1 molecular compound, TTTA·Cu(hfac)$_2$ (Cu(hfac)$_2$ = bis(hexafluoroacetylacetonato)–copper(II)), was obtained by the reaction of stoichiometric amounts of the components in a heptane solution under nitrogen atmosphere.[22] The crystal structure is shown in Fig. 8. TTTA molecules occupy the axial positions of the elongated octahedral around the Cu(II) ion, and bridge the distance between the Cu(II) ions, resulting in an infinite zigzag chain along the b axis. While Rawson et al. have reported the mono-, di-, and tri-metallic coordination compounds of 1,2,3,5-dithiadiazolyl radicals,[23] TTTA·Cu(hfac)$_2$ is the first coordination polymer made of thiazyl radicals. While various nitronylnitroxides[24] and polynitroxyl radicals[25] are known to act as a bidentate bridging ligand and to form polymeric coordination compounds, the structure of TTTA·Cu(hfac)$_2$ clearly indicates similar chemical capability of the polycyclic thiazyl radicals. As shown in Fig. 8, the Cu(II) ion is sandwiched between two TTTA molecules, labeled A and B, at distances of 2.342 and 2.478 Å from the Cu(II) ion. The former distance is shorter by more than 0.1 Å. The molecular plane of TTTA^A is nearly orthogonal to the plane defined by the four hfac oxygen atoms, while that of TTTA^B is significantly tilted.

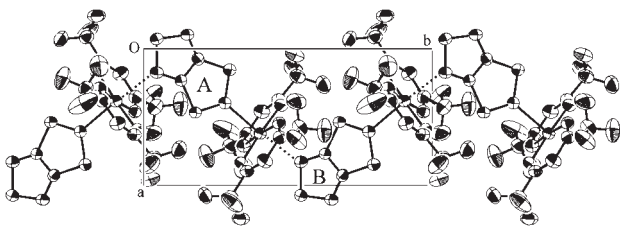

Fig. 8. The crystal structure of TTTA·Cu(hfac)$_2$.

The magnetic couplings between $Cu(hfac)_2$ and nitroxyl radicals have been previously discussed by Gatteschi et al.[24] They explained the ferromagnetic couplings in these materials in terms of the orthogonality between the $d_{x^2-y^2}$ orbital of Cu(II) and the SOMOs of the organic radicals. By analogy, it was expected that the interaction between $Cu(hfac)_2$ and $TTTA^A$ would be ferromagnetic. However, the $Cu(hfac)_2$–$TTTA^B$ interaction is probably antiferromagnetic due to the overlap between the magnetic orbitals of Cu(II) and $TTTA^B$ caused by the tilted structure.

The χ_pT value for $TTTA\cdot Cu(hfac)_2$ increases with decreasing temperature down to ca. 30 K, indicating a ferromagnetic coupling. After passing through a maximum at this temperature, χ_pT shows an abrupt decrease, suggesting a weak antiferromagnetic coupling between the ferromagnetic units. This is quite consistent with the coordination around the Cu(II) ion. The ferromagnetic coupling constant was obtained to be $J/k_B = 18.5$ K. This is stronger than those in the axial coordination compounds of $Cu(hfac)_2$ and nitroxyl radicals,[24] presumably because the energy level of the SOMO of TTTA is closer to those of the d orbitals of Cu(II).

Ferromagnetism in BBDTA Salts Driven by Evaporation of Crystal Solvent

BBDTA (=benzo[1,2-*d*:4,5-*d*′]bis[1,3,2]dithiazole) was initially reported independently by Wolmershäuser et al. and by Wudl et al.[26,27] Wolmershäuser reported the crystal structure and the ^{57}Fe Mössbauer spectra of the radical cation salt $BBDTA\cdot Fe(III)Cl_4\cdot CH_3CN$.[28] In this crystal, BBDTA forms a ladder-type structure through which the $FeCl_4$ anions are weakly linked. Mössbauer spectroscopy indicated antiferromagnetic ordering of the Fe^{3+} magnetic moments below 6.6 K. In the following section, we describe the bulk ferromagnetism in BBDTA salts driven by evaporation of the crystal solvent.

Organic Ferromagnetism with $T_C = 7$ K in BBDTA·$GaCl_4$. $BBDTA\cdot GaCl_4\cdot CH_3CN$ was prepared by the reaction of $BBDTA\cdot Cl$ and $GaCl_3$.[29] Single crystals were obtained by recrystallization from a mixed solvent of acetonitrile and dichloromethane. The structure of $BBDTA\cdot GaCl_4\cdot CH_3CN$ was found to consist of a face-to-face radical dimer, with half of the unit being crystallographically independent. The crystal solvent, CH_3CN, occupied the space beside BBDTA, coordinating to the sulfur atom. These dimers were stacked along the [110] direction via short S···N contacts, forming a ladder-type structure. Between the ladders, there was a rather short S···S contact, resulting in a 2D network parallel to the *ab* plane. The $GaCl_4$ anions were located between the ladder layers.

As shown in Fig. 9 as closed circles, the χ_pT values for $BBDTA\cdot GaCl_4\cdot CH_3CN$ are nearly zero in the whole temperature range. This nonmagnetic property can be ascribed to a strong antiferromagnetic interaction in the dimer. However, we observed a dramatic change in the bulk magnetic properties after evaporation of the crystal solvent. The open circles in Fig. 9 show the magnetic data for a sample in which 75% of the CH_3CN was removed by evacuation for 96 h. The material exhibited paramagnetism, in remarkable contrast to the nonmagnetic properties of the solvated form. As the temperature decreased, χ_pT increased gradually, which is indicative of ferromagnetism. Below 10 K, χ_pT increased rapidly, reaching

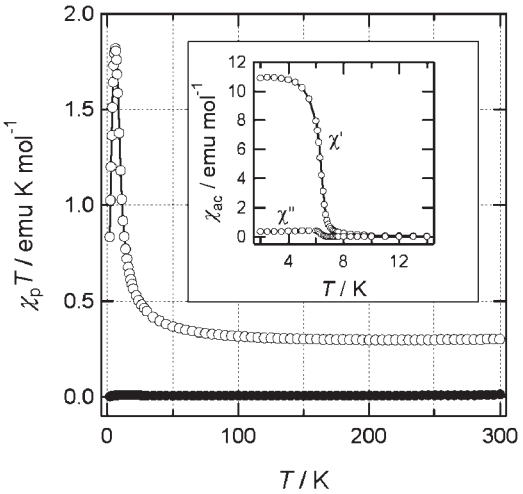

Fig. 9. Temperature dependence of χ_pT for $BBDTA\cdot GaCl_4$ in the solvated (●) and non-solvated form (○). The inset shows the temperature dependence of χ_{ac} for the non-solvated form.

1.82 emu K mol^{-1} at 6 K. The data above 50 K were fitted to the Curie–Weiss law with $\theta = 11$ K and $C = 0.28$ emu K mol^{-1}, in which the molar unit was defined as $BBDTA\cdot GaCl_4\cdot 0.25CH_3CN$. This Curie constant can be well explained by assuming that 75% of the $BBDTA\cdot GaCl_4$ exhibited paramagnetism. The inset in Fig. 9 shows the temperature dependence of the ac susceptibilities (χ': in-plane and χ'': out-of-plane) for the same sample. The plots of χ'' show an anomaly below 6.7 K with a rapid increase in χ', indicating ferromagnetic ordering. The isothermal magnetization curve at 2 K for this sample showed an abrupt increase at lower fields followed by quick saturation above 400 Oe. The value of the saturation magnetization M_s, 4310 erg Oe^{-1} mol^{-1}, agreed with the Curie constant obtained in the χ_p measurements. The presence of a negligibly small hysteresis loop with a width of less than 10 Oe indicated that the material obtained was a soft magnet.

The crystal growth of the solvent-free $BBDTA\cdot GaCl_4$ was also successful.[30] The crystals were prepared by recrystallization from a 1:1 mixed solvent of trimethylacetonitrile and dichloromethane at −23 °C. In the recrystallization, a mixture of at least three polymorphs of solvent-free $BBDTA\cdot GaCl_4$, labeled α (plates), β (needles), and γ (blocks), were obtained. The amount of the γ-phase obtained was much less than the other amounts. The three phases were distinguishable under a microscope. The α and β crystals comprised side-by-side and head-to-tail dimers, respectively, and showed diamagnetic properties at low temperatures. The magnetic behavior and crystal structure of the γ-phase was totally different; this phase exhibited a ferromagnetic transition at 7.0 K, suggesting that the desolvated material obtained from $BBDTA\cdot GaCl_4\cdot CH_3CN$ would be in the γ-phase. The crystal structure of the γ-phase consisted of a 1D zigzag chain of BBDTA formed by intermolecular and interatomic S···N contacts. Despite these short contacts, an orthogonal relation was expected between the neighboring SOMOs, reflecting the antibonding character of the SOMO in the S–N bonding.

Organic–Inorganic Hybrid Ferrimagnetism with $T_C = 44$ K in BBDTA·$FeCl_4$. $BBDTA\cdot FeCl_4\cdot CH_3COCH_3$ exhib-

ited similar solvation effects: It showed ferrimagnetic ordering at $T_N = 44$ K upon evaporation of the volatile crystal solvent, acetone.[31] In the BBDTA·$FeCl_4$·CH_3COCH_3 crystal, the BBDTA cations formed a ladder-type network that closely resembled that in BBDTA·$GaCl_4$·CH_3CN. The counter anion $FeCl_4$ formed a honeycomb network with short Cl···Cl contacts in the range of 3.62–3.85 Å. In addition, there were several short S···Cl contacts between BBDTA and $FeCl_4$, in the range of 3.28–3.66 Å, forming a three-dimensional network. The magnetic measurements on the solvated sample revealed Curie paramagnetism caused by the $S = 5/2$ Fe(III) ions at high temperatures. The contribution from BBDTA cations was thought to be negligible due to a strong antiferromagnetic interaction in the BBDTA dimer. Below 6.2 K, the χ_p values exhibited a characteristic change, indicating antiferromagnetic ordering in the $FeCl_4$ network. By contrast, the desolvated sample exhibited a significant enhancement of magnetization below 44 K, suggesting magnetic ordering at this temperature. The spontaneous magnetization observed at 2 K was very close to the theoretical value for the ferrimagnetic ordering.

The spin state of Fe^{3+} in the desolvated material was evaluated based on ^{57}Fe Mössbauer measurements at 20 and 50 K.[31] The spectrum at 50 K indicated the presence of high-spin Fe(III) ions. At 20 K, a series of new Zeeman split peaks (internal magnetic field = 21.9 T) with intensity ratios of 3:2:1:1:2:3 appeared, supporting magnetic ordering of the Fe(III) ions.

BBDTA·$FeCl_4$·CH_3COCH_3 was shown to exhibit a dramatic change in magnetism after removal of the crystal solvent. Whereas the solvated material exhibited paramagnetic behavior with antiferromagnetic ordering at 6.3 K, the desolvated material included a ferrimagnetic phase with $T_N = 44$ K. This is much higher than the transition temperatures of the parent materials: 7 K for the ferromagnetic transition in BBDTA·$GaCl_4$[29] and 3 K for the antiferromagnetic transition in $(C_2H_5)_4N$·$FeCl_4$.[32] A strong antiferromagnetic coupling between the magnetic moments on BBDTA and $FeCl_4$ is thought to afford this organic/inorganic hybrid system a higher ferrimagnetic transition temperature.

Network Structures in Metallo–Tetrakis(1,2,5-thiadiazole)porphyrazines

In the previous sections, we described the characteristic crystal structures and unique solid-state properties of heterocyclic thiazyl radicals. These radicals always exhibited multidimensional network structures due to π–π overlaps, S···N electrostatic contacts, and coordination bonding. Such interactions can be expected even in non-radical chemical species, e.g. thiadiazole compounds.[33]

Phthalocyanine (MPc) compounds have been studied extensively, because of their commercial applications: for example, as dyes and catalysts. They have also attracted much interest due to their electric, electro-optic, and magnetic properties.[34,35] There are two well-known crystal forms for MPc, namely α and β,[36,37] both of which consist of 1D π–π stacking columns. The intercolumnar interactions in these structures are hindered by the terminal hydrogen atoms on the benzo-rings. Such low dimensionality would be disadvantageous for 3D electrical conduction and magnetic ordering. Seeking multi-dimensional interactions, Inabe et al. studied the [$MPc(CN)_2$] series.[38–40] Ercolani et al. synthesized tetrakis(thiadiazole)porphyrazine and the corresponding metal(II) derivatives, M–TTDPz (M = H_2, Mg, Mn, Fe, Co, Ni, Cu, and Zn),[41,42] in which intermolecular and interatomic S···N contacts are highly likely to be found. In the next section, we describe the crystal structures of the M–TTDPz series and discuss their packing motifs.

Polymorphs of M–TTDPz. Single crystals of M–TTDPz (M = H_2, Fe, Co, Ni, Cu, and Zn) were obtained by sublimation under reduced pressure with continuous N_2 gas flow,[43] though growth of Mn–TTDPz crystals was unsuccessful. The structures of the crystals obtained were determined by X-ray crystallographic analyses. It is notable that X-ray quality crystals could not be grown without N_2 gas flow.

The structures of the M–TTDPz series can be broadly classified into three forms: α, β, and γ. The α form is the structure for the H_2, Ni, and Cu derivatives, while the Ni and Cu derivatives exhibited polymorphism. The α form belongs to a monoclinic $P2_1/n$ space group, in which half of the molecule is crystallographically asymmetric. The structure consists of a layered structure, of which the top view for α-Ni–TTDPz is shown in Fig. 10a. The layer is formed by 2D hexagonal close packing of α-Ni–TTDPz with very short S···N contacts, much shorter than the sum of the van der Waals radii of N and S. These layers are stacked along the c axis by π–π interactions.

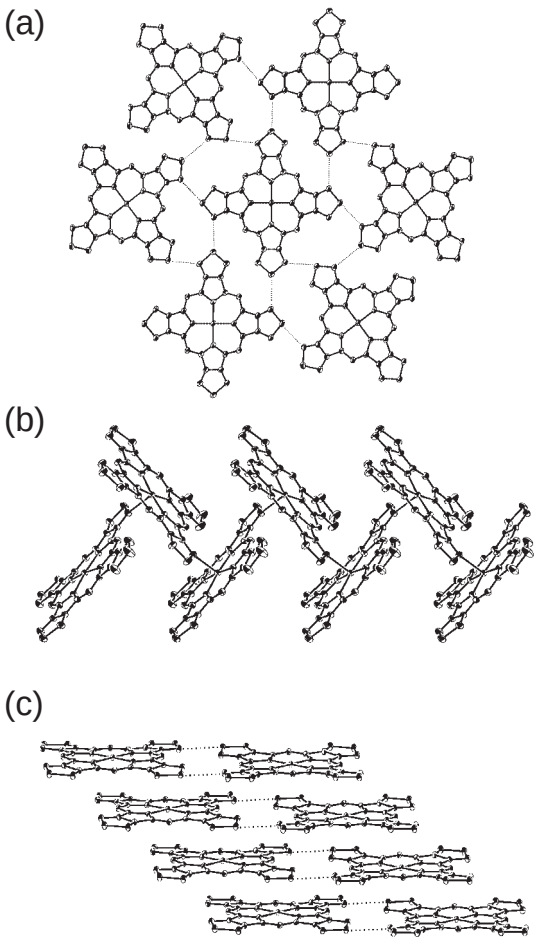

Fig. 10. Crystal structure of the M–TTDPz series: α-form (a), β-form (b), and γ-form (c).

Epitaxial growth of MPc has been studied extensively on various surfaces. It is believed that the arrangements of neighboring molecules on surfaces are governed by steric effects of the terminal hydrogen atoms on the benzo-rings.[44] By contrast, the 2D layered structure of the α form is caused by electrostatic attraction between the thiadiazole rings. This is the crucial difference between MPc and α-M–TTDPz. The 2D network observed in the case of the α form suggests that this form could be employed in the generation of oriented thin films.

The β-form, belonging to a monoclinic $P2_1/c$ space group, was found in the M = Fe, Co, and Zn derivatives. These three derivatives do not exhibit polymorphism. Figure 10b depicts the structure of β-Fe–TTDPz, which forms a 1D coordination polymer along the *b* axis. The nitrogen atom on the thiadiazole ring occupies the axial position of the metal ion in each neighboring molecule, and thus the metal ions are penta-coordinated. Each neighboring molecule in this chain is related by a two-fold screw axis parallel to the *b* axis. This type of edge-to-face interaction has previously been reported for zinc derivatives of the asymmetric porphyrazine.[45] The coordination chains stack in the *bc* plane, leading to a 2D network. The interchain arrangements give rise to a face-to-face π dimer, in which the magnetic interaction is highly localized.

The γ form was found in the Ni and Cu derivatives, although they also crystallize into the α form. The γ form belongs to the monoclinic $P2_1/n$ space group, and consists of a two-legged ladder structure along the *a* axis. Figure 10c depicts a side view of this structure in γ-Ni–TTDPz. Along the leg direction, the molecular planes, tilted by about 40° with respect to this direction, stack with π–π overlap. The axial positions of the Ni ion are occupied by nitrogen atoms bridging the distance between the pyrrole rings on neighboring separate molecules. These stacking features are similar to those of the β form of MPc.[34,35] Along the row direction, the γ-Ni–TTDPz molecules have short, side-by-side S···N contacts, which are shorter than the sum of the van der Waals radii.

Packing Motifs. The structures of metal and metal-free phthalocyanines are well known to be almost independent of the central metal ions,[34,35] with their structures governed by the π–π condensation energy of the planar molecules. By contrast, the structure of the M–TTDPz series does depend on the central metal ions, and the S···N and π–π interactions of the thiadiazole ring also play a significant role in their solid structure. Since metal-free H_2–TTDPz exhibits the α form, this structure is regulated by the π–π condensation energy. Ni–TTDPz and Cu–TTDPz do not form the β structure, which is a coordination polymer structure formed by bonding between the metal ion and the axial nitrogen atom. Absence of β-Ni–TTDPz and β-Cu–TTDPz can be explained by the fact that Ni^{2+} (d^8) and Cu^{2+} (d^9) are Jahn–Teller ions, usually with an elongated axial distance or lack of axial bonding. There is no reason for H_2–TTDPz to exhibit the β form. Fe–TTDPz, Co–TTDPz, and Zn–TTDPz crystallize into only the β form, which indicates that axial bonding is a driving force in generating the β form. Since Ni–TTDPz and Cu–TTDPz exhibit polymorphism between the α and γ forms, these forms should be energetically balanced.

We conclude that the first driving force in the packing motif of the M–TTDPz series is axial coordination between the metal ion and the nitrogen on the thiadiazole ring. This bonding generates the β form. If the central metal ion does not favor short axial bonding, M–TTDPz molecules crystallize into the α or γ form.

The temperature dependence of the magnetic susceptibilities of the magnetic materials obtained, namely the M = Co (β form), Fe (β form), and Cu (α and γ forms) derivatives, indicated their weak intermolecular exchange interactions. This is probably because the metal d orbitals and HOMO of $TTDPz^{2-}$ have *gerade* and *ungerade* symmetry, respectively; the intramolecular overlaps between them are negligible, leading to the localization of d electrons. Studies on carrier doping may yield results that enable the use of the observed 3D network structures in the M–TTDPz series.

Summary

We have described our recent work on thiazyl radicals and related materials. We described the diamagnetic–paramagnetic phase transitions in TTTA and BDTA, and their novel solid-state properties, such as room-temperature magnetic bistability, photo-induced phase transition, supercooling, and superheating, which were induced by the transitions. Comparison with spin-crossover complexes brought about semi-quantitative interpretations on the transitions. Research on bistability has become a new branch in molecular magnetism. Thiazyl radicals were demonstrated to operate as building blocks for supramolecular materials, in which ferromagnetic interactions and magnetic ordering were achieved at rather high temperatures. We reported the polymorphs and crystal structures of porphyrazine derivatives annulated by thiadiazole rings, M–TTDPz. In contrast to the 1D structure of phthalocyanines, M–TTDPz exhibited a multi-dimensional structure that depended on the central metal ions.

This review article includes the results of the collaborations with Yasuhiro Nakazawa, Kazuya Saito, Michio Sorai, Masashi Takahashi, Masuo Takeda, Hiroyuki Matsuzaki, Hiroshi Okamoto, and Tamotsu Inabe. The authors are thankful for their kind support and fruitful discussions. This work was supported by Grants-in-Aid for Scientific Research from the Ministry of Education, Culture, Sports, Science and Technology, Japan.

References

1 P. Batail, *Chem. Rev.* **2004**, *104*, 4887.

2 A. F. Herbard, M. J. Rosseinsky, R. C. Haddon, D. W. Murphy, S. H. Glarum, T. T. M. Palstra, A. P. Ramirez, A. R. Kortan, *Nature* **1991**, *350*, 600.

3 K. Mukai, H. Nishiguchi, Y. Deguchi, *J. Phys. Soc. Jpn.* **1967**, *23*, 125; K. Mukai, *Bull. Chem. Soc. Jpn.* **1969**, *42*, 40; K. Awaga, T. Sugano, M. Kinoshita, *J. Chem. Phys.* **1986**, *85*, 2211.

4 K. Awaga, T. Inabe, U. Nagashima, Y. Maruyama, *J. Chem. Soc., Chem. Commun.* **1989**, 1617; M. Kinoshita, P. Turek, M. Tamura, K. Nozawa, D. Shiomi, Y. Nakazawa, M. Ishikawa, M. Takahashi, K. Awaga, T. Inabe, Y. Maruyama, *Chem. Lett.* **1991**, 1225.

5 R. T. Oakley, *Prog. Inorg. Chem.* **1988**, *36*, 299; J. M. Rawson, A. J. Banister, I. Lavender, *Adv. Heterocycl. Chem.*

1985, *62*, 137; J. M. Rawson, G. D. McManus, *Coord. Chem. Rev.* **1999**, *189*, 135; J. M. Rawson, F. Palacio, *Struct. Bonding* **2001**, *100*, 94.

6 G. Wolmershäuser, R. Johann, *Angew. Chem., Int. Ed. Engl.* **1989**, *28*, 920.

7 W. Fujita, K. Awaga, *Science* **1999**, *286*, 261.

8 W. Fujita, K. Awaga, H. Matsuzaki, H. Okamoto, *Phys. Rev. B* **2002**, *65*, 064434.

9 V. Ksenofontov, G. Levchenko, H. Spiering, P. Gütlich, J.-F. Létard, Y. Bouhedja, O. Kahn, *Chem. Phys. Lett.* **1998**, *294*, 545.

10 V. Ksenofontov, H. Spiering, A. Schreiner, G. Levchenko, H. A. Goodwin, P. Gültlich, *J. Phys. Chem. Solids* **1999**, *60*, 393.

11 Y. Galcia, V. Ksenofontov, G. Levchenko, P. Gültlich, *J. Mater. Chem.* **2000**, *10*, 2274.

12 T. Tanaka, W. Fujita, K. Awaga, *Chem. Phys. Lett.* **2004**, *393*, 150.

13 H. Matsuzaki, W. Fujita, K. Awaga, H. Okamoto, *Phys. Rev. Lett.* **2003**, *91*, 017403.

14 E. König, G. Ritter, S. K. Kulshreshtha, J. Waigel, H. A. Goodwin, *Inorg. Chem.* **1984**, *23*, 1896.

15 G. Wolmershäuser, M. Schnauber, T. Wilhelm, *J. Chem. Soc., Chem. Commun.* **1984**, 573.

16 E. G. Awere, N. Burford, R. C. Haddon, S. Parsons, J. Passmore, J. V. Waszczak, P. S. White, *Inorg. Chem.* **1990**, *29*, 4821.

17 T. Mori, H. Mori, S. Tanaka, *Bull. Chem. Soc. Jpn.* **1999**, *72*, 179.

18 W. Fujita, K. Awaga, Y. Nakazawa, K. Saito, M. Sorai, *Chem. Phys. Lett.* **2002**, *352*, 348.

19 B. Wunderlich, *Macromolecular Physics*, Academic Press, New York, **1980**, Vol. 3.

20 M. Hase, K. Uchinokura, R. J. Birgeneau, K. Hirota, G. Shirane, *J. Phys. Soc. Jpn.* **1996**, *65*, 1392.

21 H. Yasuoka, T. Imai, T. Shimizu, in *Strong Correlation and Superconductivity*, ed. by H. Fukuyama, S. Maekawa, A. P. Malozemoff, Springer-Verlag, Tokyo, **1989**, p. 254.

22 W. Fujita, K. Awaga, *J. Am. Chem. Soc.* **2001**, *123*, 3601.

23 A. J. Banister, I. May, J. M. Rawson, J. N. B. J. Smith, *Organomet. Chem.* **1998**, *550*, 241.

24 A. Caneschi, D. Gatteschi, R. Sessori, *Acc. Chem. Res.* **1989**, *22*, 392.

25 H. Iwamura, K. Inoue, N. Koga, *New J. Chem.* **1998**, *22*, 201.

26 K. A. Williams, M. J. Nowak, E. Dormann, F. Wudl, *Synth. Met.* **1986**, *14*, 233.

27 E. Dormann, M. J. Nowak, K. A. Williams, R. O. Angus, F. Wudl, *J. Am. Chem. Soc.* **1987**, *109*, 2594.

28 G. Wolmershäuser, G. Wortman, M. Schnauber, *J. Chem. Res. Synop.* **1988**, 358.

29 W. Fujita, K. Awaga, *Chem. Phys. Lett.* **2002**, *357*, 385; T. M. Barclay, A. W. Cordes, R. H. de Laat, J. D. Goddard, R. C. Haddon, D. Y. Jeter, R. C. Mawhinney, R. T. Oakley, T. T. M. Palstra, G. W. Patenaude, R. W. Reed, N. P. C. Westwood, *J. Am. Chem. Soc.* **1997**, *119*, 2633.

30 W. Fujita, K. Awaga, *Chem. Phys. Lett.* **2004**, *388*, 186.

31 W. Fujita, K. Awaga, M. Takahashi, M. Takeda, T. Yamazaki, *Chem. Phys. Lett.* **2002**, *362*, 97.

32 E. P. Edwards, C. E. Johnson, *J. Chem. Phys.* **1968**, *49*, 211.

33 M. H. Klingele, S. Brooker, *Coord. Chem. Rev.* **2003**, *241*, 119; M. Akhtaruzzaman, M. Tomura, J. Nishida, Y. Yamashita, *J. Org. Chem.* **2004**, *69*, 2953, references are there in.

34 *Phthalocyanines: Properties and Applications*, ed. by C. C. Leznoff, A. B. P. Lever, VCH, New York, **1996**, Vol. 4.

35 *The Porphyrin Handbook*, ed. by K. M. Kadish, K. M. Smith, R. Guilard, Academic Press, New York, **2003**, Vols. 17 and 19.

36 J. M. Robertson, Organic Crystals and Molecules, Cornell University Press, New York, **1953**.

37 G. Wolmershäuser, R. Johann, *Angew. Chem., Int. Ed. Engl.* **1989**, *28*, 920.

38 T. Inabe, Y. Maruyama, *Bull. Chem. Soc. Jpn.* **1990**, *63*, 2273.

39 M. Matsuda, T. Asari, T. Naito, T. Inabe, N. Hanasaki, H. Tajima, *Bull. Chem. Soc. Jpn.* **2003**, *76*, 1935.

40 T. Inabe, *J. Porph. Phthal.* **2001**, *5*, 3.

41 P. A. Stuzhin, E. M. Bauer, C. Ercolani, *Inorg. Chem.* **1997**, *37*, 1533.

42 E. M. Bauer, D. Cardarrilli, C. Ercolani, P. A. Stuzhin, U. Russo, *Inorg. Chem.* **1999**, *38*, 6114.

43 M. Fujimori, Y. Suzuki, H. Yoshikawa, K. Awaga, *Angew. Chem., Int. Ed.* **2003**, *42*, 5863; Y. Suzuki, M. Fujimori, H. Yoshikawa, K. Awaga, *Chem. Eur. J.* **2004**, *10*, 5158.

44 D. E. Hooks, T. Fritz, M. D. Ward, *Adv. Mater.* **2001**, *13*, 227; A. Yamashita, T. Hayashi, *Adv. Mater.* **1996**, *8*, 791, references are therein.

45 M. J. Cook, A. Jafari-Fini, *J. Mater. Chem.* **1997**, *7*, 2327.

Kunio Awaga was born in 1959 in Kanazawa, Japan. He graduated from The University of Tokyo in 1983, and received his D.Sc. there in 1988 under the supervision of Professor Minoru Kinoshita for some the experimental and theoretical studies on ferromagnetic intermolecular interactions. In 1988, he was appointed as a research associate at the Institute for Molecular Science, and started some studies on the nitronylnitroxide radicals, including the first organic ferromagnet *p*-NPNN, the organic *Kagome* antiferromagnet *m*-MPYNN, etc. In 1992, he returned to The University of Tokyo as an associate professor at the Department of Pure and Applied Sciences, and expanded his activity toward thiazyl radicals and organic–inorganic hybrid materials. In 2001, he moved to Nagoya University as a professor at the Department of Chemistry.

Wataru Fujita was born in Toyama, Japan in 1968. He received his B.Eng. degree in organic chemistry from Nagoya University in 1992, and then received his M.Eng. degree in analytical chemistry from Nagoya University in 1994. He obtained his Ph.D. degree in inorganic chemistry under the direction of Professor Kunio Awaga at The University of Tokyo in 1997. He then began an academic career as a research associate at The University of Tokyo. In 2001, he moved as a research associate to the Research Center for Materials Science, Nagoya University. His present research focuses on magnetic and conductive properties of various cyclic thiazyl radicals and their molecular complexes.